Macromolecules
ARTICLE

Macromolecules **2010**, *43*, 375–383 **375**
DOI: 10.1021/ma9017058

Crystallization of Poly(butylene terephthalate) from the Glass

Takashi Konishi* and Yoshihisa Miyamoto

Graduate School of Human and Environmental Studies, Kyoto University, Kyoto 606-8501, Japan

Received July 31, 2009; Revised Manuscript Received November 2, 2009

ABSTRACT: Crystallization from the glass of poly(butylene terephthalate) (PBT) has been investigated by small-angle X-ray scattering and differential scanning calorimetry. When PBT crystallizes from the glassy state, the nodule crystalline structures in nanometer scale forms and the micrometer order objects, i.e., spherulites, are not observed. The nodule size grows and saturates at a given annealing temperature and increases with increasing annealing temperature. Two temperatures are obtained by the linear extrapolation of the temperature dependence of the reciprocal nodule size to naught. The equilibrium melting temperatures by the Gibbs−Thomson plot, i.e., the melting temperature versus reciprocal nodule size, are also the same temperatures. The lower extrapolated temperature corresponds to the equilibrium melting temperature of the α-form of PBT. The higher extrapolated temperature is discussed on the basis of the Strobl crystallization model and can be regarded as the equilibrium mesophase−crystal transition temperature.

1. Introduction

Poly(butylene terephthalate) (PBT) has two triclinic crystalline forms, the α-form and the β-form.[1−7] The α-form crystalline structure is mainly obtained when PBT is crystallized from the molten state or the glassy state. The β-form structure forms when the α-form crystalline structure is held under strain, and transforms reversibly to α-form on removal of the strain. The *c*-axis (fiber axis) length of the α-crystalline unit cell, ca. 11.6 Å, is shorter than that of β-form, ca. 13.0 Å, because the conformations of four methyl groups in α- and β-forms are gauche−trans−gauche and all-trans conformations, respectively.

PBT forms a mesomorphic phase, which has an intermediate structure between crystal and amorphous, in addition to the crystalline forms when an amorphous PBT is stretched at room temperature.[8] The mesomorphic phase has been regarded as a smectic structure by the discoverer. The smectic structure transforms into α-form by heating. The length of the smectic periodicity is 11.69 Å, which corresponds to the *c*-axis length of α-crystalline unit.[8] A similar mesomorphic phase has been found in other polyesters,[9−15] isotactic polypropylene (iPP),[16−19] and syndiotactic polypropylene (sPP).[20,21] For poly(ethylene terephthalate) (PET)[9−13] and poly(ethylene naphthalate) (PEN),[14] the mesomorphic phases are formed only by stretching the glass. For poly(butylene naphthalate) (PBN),[15] iPP[16−19] and sPP[20,21] the mesomorphic phases are formed by rapid quenching from the molten state as well as by stretching in the glassy state. Such a mesomorphic phase has been also defined as conformationally disordered (condis) crystal or solid mesophase.[22] In this report, a mesomorphic phase is called a smectic structure.

For PBT two glass transition temperatures, T_g, have been reported as 41 and 102 °C by temperature-modulated differential scanning calorimetry (TMDSC).[23] The lower and the higher T_g's are defined as those of a mobile-amorphous, i.e., a normal liquid, T_g^{moblie}, and a rigid-amorphous fraction, T_g^{RAF}, respectively. A rigid-amorphous fraction exists around the crystallites below T_g^{RAF} and is related to the stress transmitted across the crystal to amorphous interface.[23] A rigid-amorphous fraction disappears above T_g^{RAF}.

The crystallization mechanism of PBT has been studies by many methods.[23−33] For example, Hsiao reported the isothermal crystallization in PBT from the melt by the time-resolved simultaneous small-angle X-ray scattering (SAXS) and wide-angle X-ray diffraction (WAXD) methods.[31] Because the crystallization rate of PBT is faster than that of PET,[23,32] however, the behavior of the crystallization mechanism at a large quenching depth and the crystallization mechanism from the glass has not been clarified. In the case of iPP, the spherulites appear on crystallization from the molten state. The molten iPP transforms into the smectic structure by quenching to 0 °C, and the morphology of the smectic structure is a so-called "nodule" structure whose diameter is ca. 100 Å at room temperature.[33−35] The obtained film of the smectic iPP is transparent. The smectic structure transforms into α-crystalline form of the nodular morphology by heating.[33−36] The nodule size grows and saturates at a given crystallization temperature, T_c, and increases with increasing annealing temperature.[36] Thus, the formation of spherulites is inhibited in the crystallization process of iPP from the smectic structure.

Recently Strobl has proposed an improved crystallization model through a transient mesomorphic phase.[37,38] According to the model, when a polymer material crystallizes from the molten state, first granular domains of mesomorphic phase form, then transform into the crystalline domains and finally form the lamellar structure. The model also predicts that the extrapolation of temperature dependence of the size of crystal gives a virtual transition between the mesomorphic phase and the crystal, and that the equilibrium mesomorphic−crystal transition temperature, T_{MC}^{∞}, is located above the equilibrium melting temperature of crystal, T_m^{∞}.[38] In order to clarify the crystallization mechanism of PBT which forms the smectic structure by stretching at a large quenching depth, we have investigated the crystallization from the glass of PBT by SAXS and differential scanning calorimetry (DSC). In this report, we obtain T_m^{∞} from the relation between T_m and the size of crystallite by SAXS and DSC and discuss whether Strobl's model is applicable to the crystallization mechanism of PBT from the glass in the present experimental results.

*Corresponding author. E-mail t.konishi@kt5.ecs.kyoto-u.ac.jp. Telephone: +81-75-753-6775. Fax: +81-75-753-6805.

Published on Web 12/08/2009

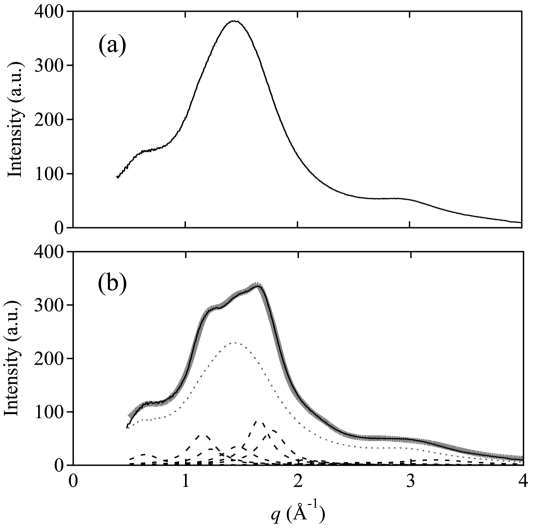

Figure 1. WAXD of (a) the quenched PBT and (b) the PBT annealed at 30 °C for 30 min from the quenched state. The solid line in (b) shows the observed intensity and the thick gray line, the fitting curve. The latter is reproduced by summing up the components of the α-form (broken line) and amorphous phase (dotted line).

2. Experimental Section

The polymer used in this study was PBT with M_v = 38 000 purchased from Sigma-Aldrich Co. Ltd. PBT was melted at ca. 280 °C for 2 min on a hot-plate, and then rapidly quenched in ice−water. The thickness of the quenched PBT film is ca.150 μm. The quenched PBT film was measured by wide-angle X-ray diffraction (WAXD) immediately after quenching. The PBT film annealed at 30 °C for 30 min heated from 0 °C was also measured by WAXD. The time-resolved SAXS measurements were carried out in the heating process and the isothermal crystallization process for the quenched PBT. In the heating process the PBT sample was heated from 30 to 260 °C at a rate of 10 °C/min after annealing at 30 °C for 5 min. In the isothermal crystallization the PBT samples were heated from room temperature at the rate of 100 °C/min, and then were isothermally crystallized at T_c=40, 60, 80, 100, 120, 140, 160, 180, and 200 °C. In order to ensure the scattering intensity the sample films were plied 2-fold. The heating process of PBT sample after annealing at T_c (30 − 225 °C) for t_c (5 - 120 min) was analyzed by DSC for comparison with the SAXS measurements.

WAXD measurements were performed using the Rigaku Rint 2500 system. The WAXD patterns were recorded using an imaging plate which covers the q-range from 0.4 to 4 Å^{-1} (q = $4\pi(\sin\theta)/\lambda$; λ and 2θ being X-ray wavelength and scattering angle, respectively). The value of λ in WAXD was 1.54 Å^{-1}. SAXS measurements were performed using the beamline BL-45XU at SPring-8, Nishiharima, Japan. The SAXS covers the range of scattering vector q from 0.08 to 0.2 Å^{-1}. The value of λ in SAXS was 0.9 Å^{-1}. The temperature of the samples for the SAXS measurements was controlled using a Linkam LK-600PH. The DSC measurement was carried out in the heating process of the PBT samples with Shimadzu DSC60 at a rate of 10 °C/min in the range from −10 to +280 °C.

3. Results and Discussion

3.1. Structures of PBT Crystallized from the Glass. Figure 1 shows the WAXD diagrams of the PBT quenched from the molten state to 0 °C and the PBT's annealed at 30 °C for 30 min from the quenched state. The structure of the PBT as quenched is identified as the amorphous phase because of the existence of an amorphous halo only. The PBT annealed at 30 °C has a fraction of α-form because the broad Bragg peaks of α-form at q=0.64, 1.15, 1.22, 1.46, 1.65, 1.77, 2.05, 2.20, and 3.22 Å^{-1} are

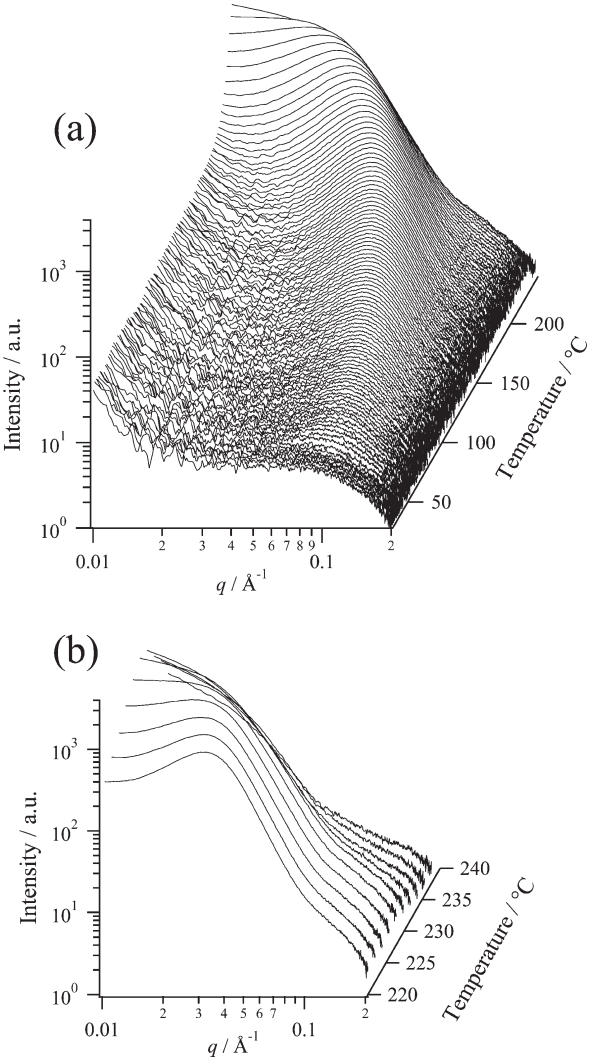

Figure 2. SAXS profiles of a heating process for the PBT annealed at 30 °C for 30 min from the quenched state at a rate of 10 °C/min: (a) from 30 to 220 °C; (b) from 220 to 240 °C.

observed in Figure 1b. The peaks were fitted to the Lorentzian functions. The crystallinity of the annealed PBT in Figure 1b was calculated using an area ratio of the sum of the fitting peaks to the observed diagram and was obtained as 35%. The annealed PBT film is transparent despite crystallization. Micrometer order objects, i.e., spherulites, are not observed during the heating process from the glass to the melt by an optical microscope. Thus, the crystallization from the glass of PBT forms the nanometer order objects, i.e., the nodular structure, rather than spherulites composed of lamellar crystals.

Figure 2 shows the SAXS intensities $I(q)$ of the quenched PBT during the heating process from 30 to 260 °C. The SAXS curve at 30 °C has a weak peak at $q_{max} \approx 0.09$ Å^{-1}, corresponding to ca. 70 Å. According to the WAXD results, already the PBT annealed 30 °C is semicrystalline. Therefore, the observed SAXS peak is related to a nanoscale correlation among the corresponding entities and the entities are crystalline. The ensemble of nanoscale entities is regarded as a nodule structure similar to the one which is observed in iPP quenched from the melt to 0 °C.[33−35] Manabe and coworkers have studied the morphology of PBT isothermally crystallized at 40 °C from melt by transmission electron microscopy.[39] They have observed granule-like crystalline domains with indistinct boundary in the PBT sample.

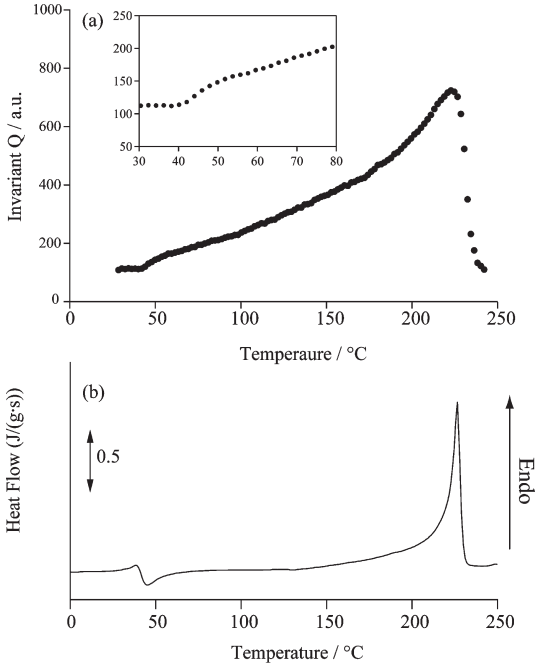

Figure 3. (a) Temperature dependence of invariant Q calculated from the results of the SAXS profiles in Figure 2. (b) DSC curve of a heating process at a rate of 10 °C/min for the PBT annealed at 30 °C for 30 min from the quenched state.

The peak shifts to the lower q side and the intensity I_{max} at q_{max} increases with increasing annealing temperature.

In order to clarify the structural change during the heating process, we calculate the invariant Q defined by[40]

$$Q = \int_0^\infty 4\pi q^2 I(q)\, dq = (\rho_c - \rho_a)^2 \phi_c (1 - \phi_c) \qquad (1)$$

where ϕ_c is crystallinity, and ρ_c and ρ_a are the densities of crystal and amorphous, respectively. Figure 3a shows the invariant Q calculated from the SAXS results in Figure 2. The Q value remains nearly constant below 40 °C, increases from 40 to 224 °C, and then decreases. The behavior of the Q shows that the PBT further crystallizes from 40 °C and the crystalline structure melts at 224 °C during the heating process of the PBT annealed at 30 °C from the glassy state. Figure 3b shows the DSC curve of the heating process of the quenched PBT annealed at 30 °C for 30 min in order to compare to the behavior of the Q value. The curve shows endothermic peaks at 38 and 226 °C and an exothermic peak at 45 °C. The peak at 226 °C is obviously identified as the melting peak and corresponds to the value of T_m from the behavior of the Q value. The endothermic and exothermic peaks at 38 and 45 °C have been identified as the melting peak and the crystallization peak to α-form, respectively.[32] These peaks shift to higher temperature positions with increasing annealing temperature.[32]

3.2. Change in Nodule Structure Size and the Equilibrium Melting Temperature. The morphology of crystalline part in a semicrystalline polymer material is usually observed as a lamellar structure. The melting temperature T_m of the crystal depends on the lamellar thickness l and the relationship between T_m and l is given by[40]

$$l^{-1} = \Delta H(T_m^\infty - T_m)/2\delta_e T_m^\infty \qquad (2)$$

where ΔH, T_m^∞, and δ_e are the heat of fusion, the equilibrium melting temperature and the specific energy of chain-folded surface, respectively. Furthermore, it is well-known that the lamellar thickness l also depends on a crystallization temperature T_c, and from theoretical,[41] experimental,[42−45] and simulation[46,47] evidence the relationship between T_c and l is given by

$$l^{-1} \sim (T_c^\infty - T_c) \qquad (3)$$

where T_c^∞ denotes a temperature at which an infinite lamellar thickness forms.

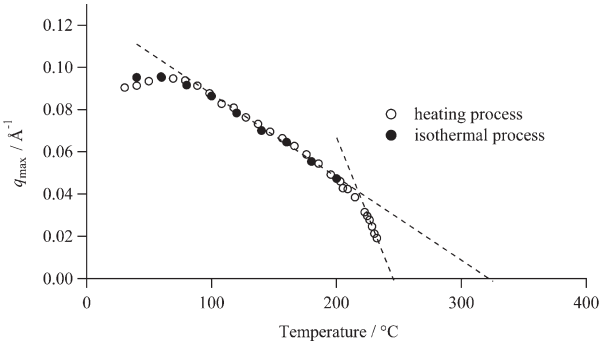

Figure 4. Temperature dependence of q_{max} obtained from the SAXS results in the heating process (open circles) and the isothermal process (closed circles).

Figure 4 shows the temperature dependence of the q_{max} of SAXS curves in Figure 2. During the heating process of the quenched PBT, q_{max} slightly increases until 70 °C, decreases above 70 °C, and then decreases more drastically above 210 °C. The values of q_{max} in the high temperature region from 210 to 230 °C are extrapolated to 245 °C, which well corresponds to the T_m^∞ reported by Chen and co-workers.[32]

A scattering function for a system of dispersed particles is described by the product of structure factor and form factor. The value of q_{max} is generally given by the combination of the internodule distance Λ and the nodule size d. When the scatterers are densely packed in space as suggested by the crystallinity of 35% in the present case, however, q_{max} is approximately given by

$$q_{max} \approx 2\pi/\Lambda \qquad (4)$$

Parts a and b of Figure 5 show the SAXS profiles during the heating process normalized by q_{max} and I_{max}. The normalized SAXS profiles at all temperatures in Figure 5a do not give a master curve, but those between 100 and 200 °C in Figure 5b give a master curve. When the scattering functions normalized by q_{max} and I_{max} give a master curve, the structures are similar. Therefore, the nodule structures between 100 and 200 °C can be scaled by Λ, which indicates that the ratio of d to Λ and hence ϕ_c is constant in this temperature range. The increase in Q between 100 and 200 °C can be interpreted in terms of the difference in the thermal expansion coefficients between crystal and amorphous phase, i.e., the factor $(\rho_c - \rho_a)^2$ in eq 1.[4,24,30] Here, we will apply eq 3 to the case of the nodule structure by substituting q_{max} for l^{-1} (see section 3.5):[36]

$$q_{max} \sim (T_c^\infty - T_c) \qquad (5)$$

In Figure 4, a straight line can be drawn from the temperature dependence of q_{max} between 100 and 200 °C and is extrapolated $T_c^\infty = 330$ °C, which is 85 °C higher than T_m^∞. Here $T_c^\infty = 330$ °C is obtained from the temperature dependence of d between 100 and 200 °C and $T_m^\infty = 245$ °C is obtained from that of Λ above 220 °C. The crossing point of

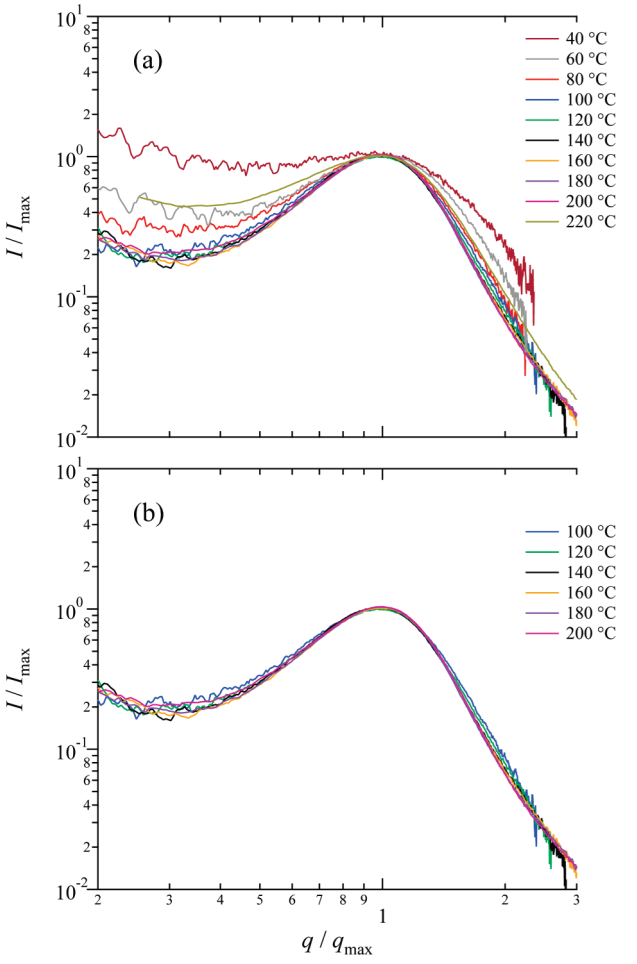

Figure 5. SAXS profiles normalized by q_{max} and I_{max} collected during the heating process of the quenched PBT at a rate of 10 C/min in the temperature ranges (a) from 40 to 220 °C and (b) from 100 to 200 °C.

two straight lines drawn from the temperature dependence of q_{max} below 200 °C and above 220 °C in Figure 4 is 215 °C.

We examined the SAXS behavior in the isothermal process of the quenched PBT in order to compare to the q_{max} value of the heating process of the quenched PBT. Parts a and b of Figure 6 show the time evolved SAXS curves during the isothermal process at 40 and 140 °C from the glassy state, respectively. The SAXS curves at annealing temperatures higher than 80 °C show that the q_{max} slightly shifts to the lower q-value region immediately after starting annealing and then remains constant, and the intensity I_{max} at q_{max} increases with time. Figure 7 shows the annealing time dependence of q_{max} and I_{max} of SAXS profiles during the isothermal processes at 40, 60, 80, 100, 120, 140, 160, 180, and 200 °C. The q_{max} of isothermal process at 40 °C increases gradually with time. The q_{max} at 60 °C also increase gradually with time but faster than that at 40 °C. However, the q_{max} at each annealing temperature above 60 °C immediately shifts to the value determined by the temperature and remains unchanged within the annealing time in the present measurements. The I_{max} of SAXS profile at each annealing temperature also increases up to a value dependent on temperature. This characteristic behavior suggests the existence of a quasi-equilibrium state for the relation between the nodule structure size and annealing temperature. Such a behavior has been observed in the isothermal crystallization process of iPP from room temperature in which iPP has the smectic

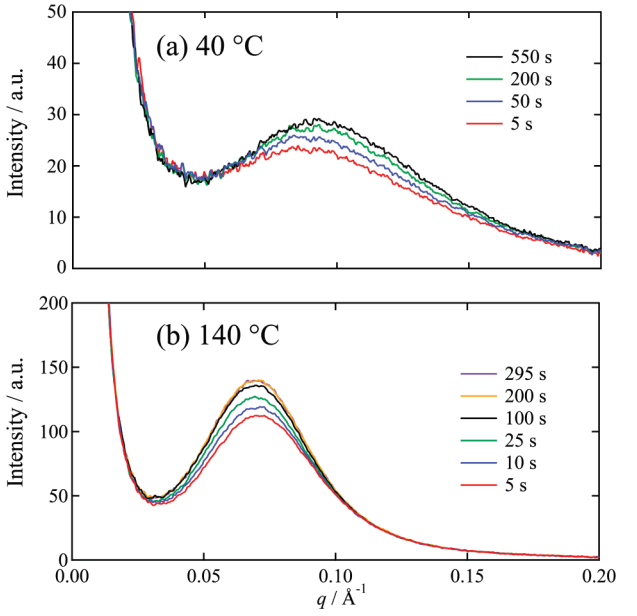

Figure 6. Time-resolved SAXS profiles of the PBTs annealed at (a) 40 and (b) 140 °C from the quenched state.

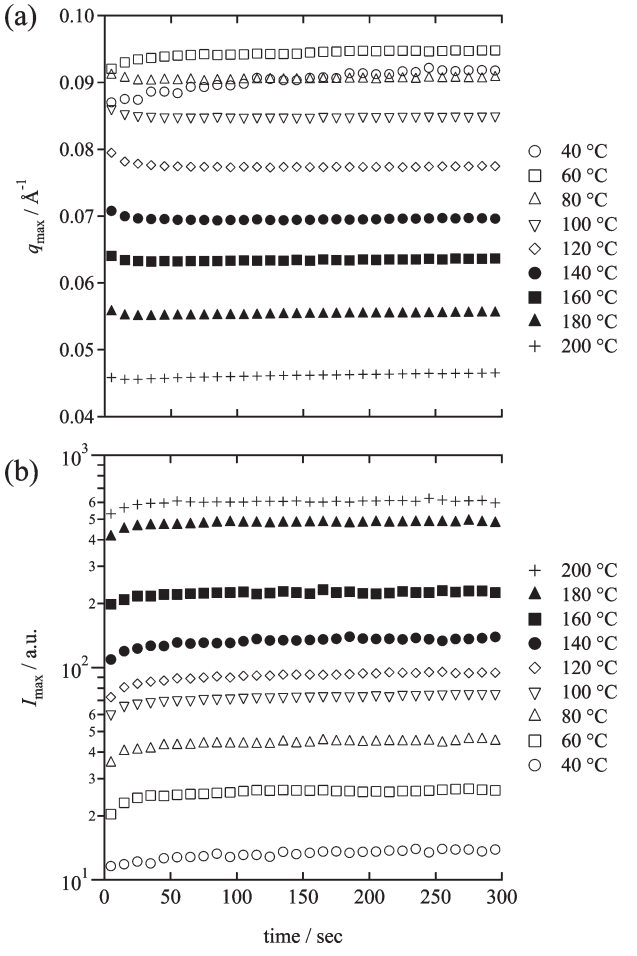

Figure 7. Time evolutions of (a) q_{max} and (b) I_{max} obtained from SAXS profiles of the PBT annealed at several temperatures from the quenched state.

structures.[36] The rate of change in I_{max} is slightly slower than that in q_{max} for all annealing temperatures. The q_{max} of SAXS profiles of the PBTs annealed at 40 and 60 °C for

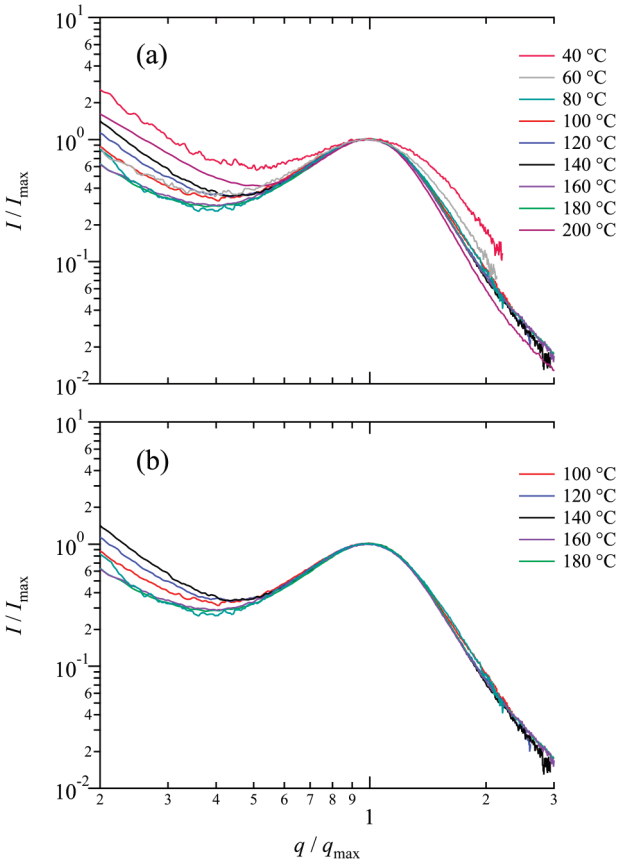

Figure 8. SAXS profiles normalized by q_{max} and I_{max} for the PBT annealed at different temperatures for 200 s from the quenched state. The temperature ranges are (a) 40 to 200 °C and (b) 100 to 180 °C.

600 s and at 80, 100, 120, 140, 160, 180, and 200 °C for 200 s are plotted in Figure 4. The q_{max} in the isothermal processes above 80 °C are the same as those in the heating process.

Parts a and b of Figure 8 show the normalized SAXS profiles during the isothermal process at different temperatures in the range between 40 and 200 °C and between 100 and 180 °C at 200 s normalized by q_{max} and I_{max}. Although the normalized SAXS profiles in Figure 8a do not give a master curve, the normalized SAXS profiles in Figure 8b superpose except at low q. The result equally leads that the q_{max}^{-1} is proportional to d between 100 and 180 °C in the isothermal process as in the heating process (Figure 5, parts a and b). $T_c^{\infty} = 330$ °C is also obtained from the SAXS results in both the heating process and the isothermal process.

3.3. The Melting Temperature of the Nodule Structure and the Equilibrium Melting Temperature. Figure 9 shows the DSC curves of the heating process of the PBT annealed at T_c for $t_c = 10$ min from the glass. The DSC curves of the PBT specimen annealed below 215 °C show two endothermic peaks. As mentioned above, the endothermic peaks are identified as the melting peaks. Figure 10 shows the relation between two melting temperatures T_m and crystallization temperature T_c. The lower melting temperature exists just above the annealing temperature between 40 and 220 °C. Similar results are reported by Cheng and co-workers.[32] The higher melting temperature might be obtained by the second crystallization during the heating process. Furthermore, from the T_m values above the 215 °C the T_m^{∞} value is obtained as 245 °C which corresponds to that reported by other research groups.[32]

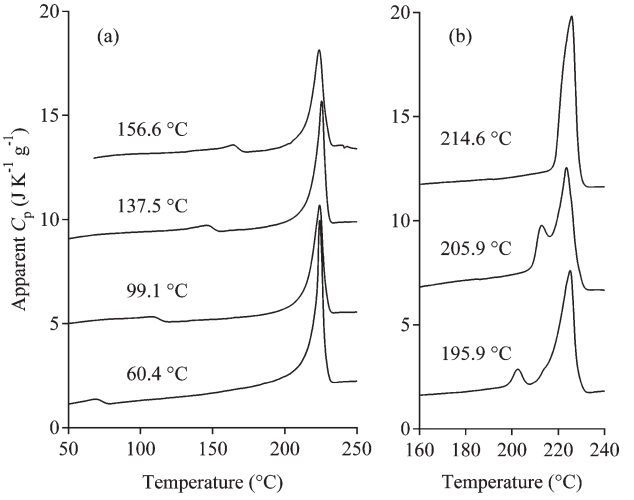

Figure 9. DSC curves in the heating process at a rate of 10 °C/min for the PBT annealed at several temperatures for 10 min from the quenched state. The inserted numbers indicate the annealing temperatures, T_c. The DSC curves are shifted vertically.

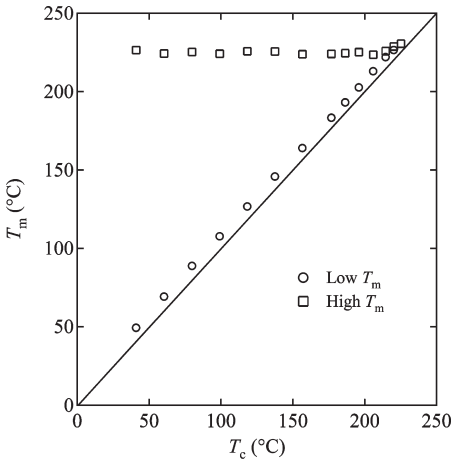

Figure 10. T_c dependence of the low and high T_m's obtained from the DSC curves in Figure 9 in the heating process for the PBT annealed at T_c for 10 min from the quenched state.

The SAXS results show that the nodule size is inversely proportional to the q_{max} value between 100 and 180 °C (Figures 4 and 8). Thus, the melting temperature, $T_{m,n}$, of the nodule structure formed by annealing between 100 and 180 °C can be obtained as lower T_m in Figure 10, and the equilibrium melting temperature can be estimated by eq 2, i.e., the Gibbs−Thomson plot. Figure 11 shows the relation between the relative reciprocal nodule size defined by q_{max} and T_m. The nodule size on crystallization at T_c in DSC measurements is estimated from the SAXS result in Figure 4. The extrapolated temperature is $T_m^{\infty} = 333$ °C and corresponds to the value of T_c^{∞}, 330 °C, obtained from the SAXS results. However the T_m^{∞} = ca. 330 °C differs substantially from $T_m^{\infty} = 245$ °C in Figure 11. The reason for the difference will be discussed subsequently.

3.4. The Crystalline Morphology below 100 °C and above 200 °C. From the SAXS results the nodule structure can not be scaled by Λ below 100 °C and above 200 °C. As shown in Figure 10 presenting the relation between T_c, $T_{m,n}$ (lower T_m), and T_m of the crystallite (higher T_m), for all T_c the $T_{m,n}$ is only slightly above T_c. This means that even for temperatures below 100 °C the nodule size d increases with increasing

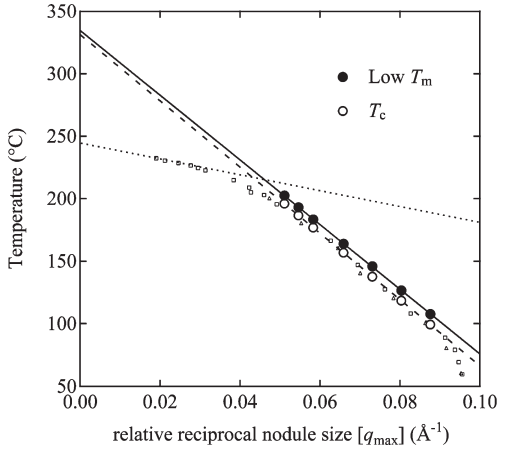

Figure 11. Relation between relative reciprocal nodule size and crystallization temperature T_c (open circles) and low T_m (filled circles). The relative nodule size obtained by the isothermal process at T_c is estimated from the SAXS result (Figure 4) and the relative reciprocal nodule size is displayed as q_{max} in the figure. Small squares and triangles present the q_{max} values in the heating process and the isothermal crystallization process in Figure 4, respectively.

T_c. However Figure 4 shows the q_{max} value almost remains unchanged below 100 °C. The results explain that the internodule distance Λ remains in spite of the increase in the nodule size d. Pyda and co-workers have reported that T_g^{RAF} is located at 102 °C.[23] The rigid-amorphous fraction is less mobile layer surrounding the crystal and inhibits a nucleation of a crystal. We consider that Λ is not proportional to d because the rigid-amorphous fraction that inhibits the nucleation of the nodules exists as the excess space around the nodule structure below $T_g^{RAF} = 102$ °C. Above the T_g^{RAF}, the rigid-amorphous fraction disappears, the nucleation occurs and the nodule structures can be scaled by SAXS.

Next we discuss the melting behavior above 200 °C. Figure 12a shows the DSC curves of PBT annealed at $T_c = 205$ °C for several t_c. The lower T_m increases with t_c (Figure 12b). From the DSC result, d is considered to increase with t_c in the isothermal process above 200 °C in order to decrease the specific surface of the nodule structures. Thus, we suggest that the reason why the normalized SAXS profiles above 200 °C in Figures 5 and 8 do not give a master curve is the increase in the ratio of d to Λ.

3.5. A Crystallization Model through a Metastable State for a Polymer Consisting of a Nodule Structure. We discuss a crystallization model applicable to the experimental results of PBT having the nodule structure and two extrapolated equilibrium temperatures. Keller and co-workers have presented the orthorhombic crystalline formation of polyethylene (PE) through the hexagonal phase by the thermodynamic treatment.[48,49] At a temperature below the melting temperature of the orthorhombic phase under a pressure below the triple point, the orthorhombic phase is stable and the hexagonal one is metastable. At this temperature and pressure, a crystal first grows in the hexagonal phase, and then the hexagonal phase transforms into the orthorhombic phase when the thickness of the hexagonal phase reaches a thickness thermodynamically stable for the orthorhombic phase. A hypothetical equilibrium transformation temperature T_{tr} can be estimated higher than T_m^{∞} of the orthorhombic phase.

Strobl and co-workers[37,38] modified the Keller's treatment and proposed an improved crystallization model through a transient mesomorphic phase based on the experimental evidence[43−45] of syndiotactic polypropylene (sPP),

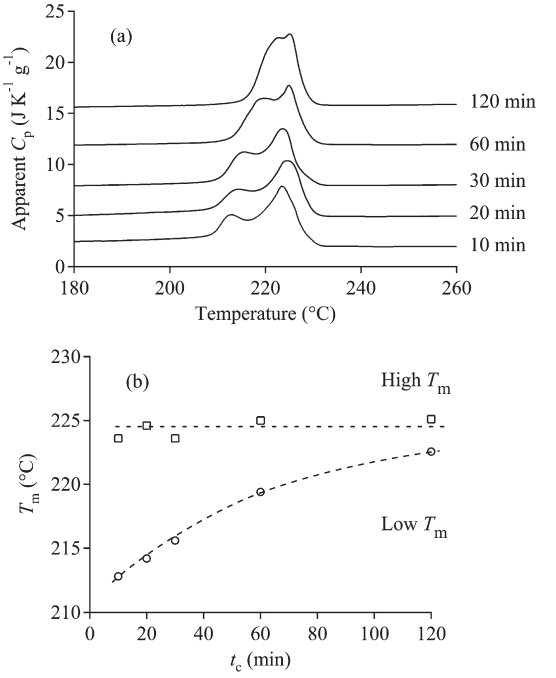

Figure 12. (a) DSC curves of a heating process at a rate of 10 °C/min for the PBT annealed at 205 °C for t_c = 10, 20, 30, 60, and 120 min from the quenched state. The DSC curves are shifted vertically. (b) t_c-dependences of peak positions of high and low T_m's in part a.

poly(ε-caprolactone), PE and isotactic polypropylene (iPP). The model explains the growth mechanism of crystalline lamellae through the mesomorphic phase:[37,38] (i) The mesomorphic layers form on the growth front of lamellae. (ii) When the mesomorphic layer grows up to a critical size, the mesomorphic layer transforms into the granular crystalline blocks. (iii) The crystalline blocks merge together and finally form the lamellar structure. The model also proposes the existences of the melting temperature of the mesomorphic phase, T_{am}, and a virtual transition temperature between the mesomorphic and the crystalline phase, T_{mc}.[38]

Here we modify Strobl's model to comply with the nodule structures obtained from the experimental results of PBT. We consider the whole growth mechanism of the nodule structures which exist all over the sample instead of the local growth mechanism on the growth front of lamellar structures. The present crystallization model assumes that the nodule structure grows when the nodule structure is in the mobile mesomorphic phase, and stops growing when the mesomorphic phase transforms into the rather immobile crystalline phase. At a high temperature near T_m^{∞}, however, the crystallization model allows that the crystalline nodule structure further gradually grows in order to decrease the specific surface of the nodule structures.

Figure 13 shows a schematic plot of the free energy, G, versus temperature, T, at an ambient pressure for the system having the mesomorphic phase as a metastable state. The subscripts L, M and C denote the liquid, the mesomorphic and the crystalline phase, respectively in the following discussion. The free energies, G_M and G_C are dependent on a nodule size, d. When the nodule structure is infinite $d = d_\infty$, the differences between the free energies G_L and G_C, between G_L and G_M and between G_M and G_C at a temperature T ($T < T_{MC}$) are given by

$$\Delta G_{LC}(d_\infty) = G_C(d_\infty) - G_L = -\Delta H_{LC}(T_{LC}^{\infty} - T)/T_{LC}^{\infty} \quad (6)$$

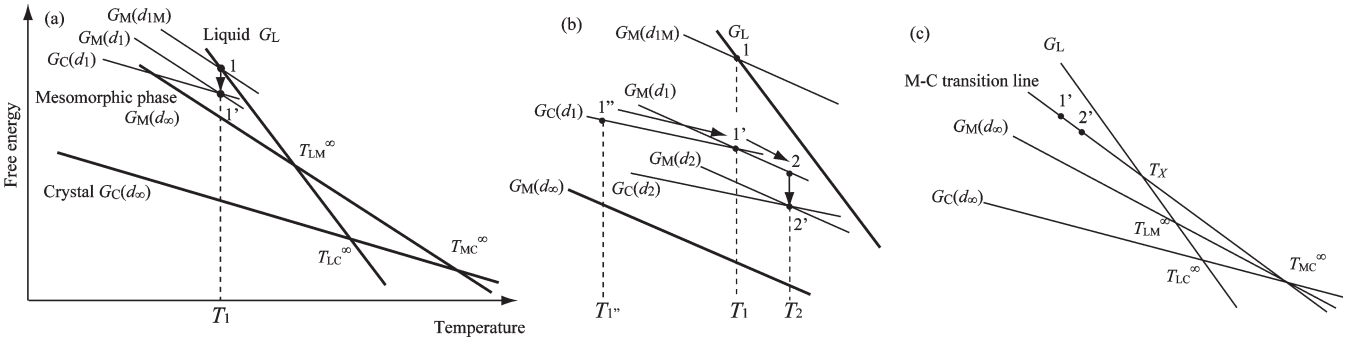

Figure 13. Schematic relationship between free energy G and temperature T for the crystalline polymer system having a metastable mesomorphic phase. The free energies of liquid, mesophase and crystal are denoted as G_L, G_M, and G_C, respectively. $G_M(d)$ and $G_C(d)$ are the free energies with a nodule size d. d_∞ is an infinite size and d_1 and d_2 are the crystalline nodule size at T_1 and T_2, respectively (d_∞ (infinite) > d_2 > d_1). Temperatures of cross-points of $G_L - G_C(d_\infty)$, $G_L - G_M(d_\infty)$, and $G_M(d_\infty) - G_C(d_\infty)$ are the equilibrium transition temperatures T_{LC}^∞, T_{LM}^∞, and T_{MC}^∞. Key: (a) survey of the free energy diagram, (b) enlarged diagram around the point 1 in part a, and (c) M−C transition line located in part a.

$$\Delta G_{LM}(d_\infty) = G_M(d_\infty) - G_L = -\Delta H_{LM}(T_{LM}^\infty - T)/T_{LM}^\infty \quad (7)$$

$$\Delta G_{MC}(d_\infty) = G_C(d_\infty) - G_M(d_\infty) = -\Delta H_{MC}(T_{MC}^\infty - T)/T_{MC}^\infty \quad (8)$$

where ΔH_{LC}, ΔH_{LM}, and ΔH_{MC} are the heats of L−C, L−M, and M−C transitions, respectively, and T_{LC}^∞, T_{LM}^∞ and T_{MC}^∞ are the equilibrium L−C, L−M, and M−C transition temperatures, respectively. When d is finite, $\Delta G_{LC}(d)$ and $\Delta G_{LM}(d)$ are given by

$$\Delta G_{LC}(d) = A_d\delta_{LC} - V_d\Delta H_{LC}(T_{LC}^\infty - T)/T_{LC}^\infty \quad (9)$$

$$\Delta G_{LM}(d) = A_d\delta_{LM} - V_d\Delta H_{LM}(T_{LM}^\infty - T)/T_{LM}^\infty \quad (10)$$

where A_d and V_d are specific surface and specific volume, respectively, of the nodule structure having d, and δ_{LC} and δ_{LM} are surface free energies of L−C and L−M interfaces, respectively. Noted that the $G_C(d)$ and $G_M(d)$ increase with decreasing d and the rate of increase in of $G_C(d)$ is larger than that of $G_M(d)$ because $\delta_{LC} > \delta_{LM}$ is expected. From eq 6 − 10, the free energy difference between mesophase - crystal is given by

$$\Delta G_{MC}(d) = A_d\delta_{MC} - V_d\Delta H_{MC}(T_{MC}^\infty - T)/T_{MC}^\infty \quad (11)$$

where

$$\begin{aligned}\delta_{MC} &= \delta_{LC} - \delta_{LM}\\ \Delta H_{MC} &= \Delta H_{LC} - \Delta H_{LM}\\ \Delta H_{MC}/T_{MC}^\infty &= \Delta H_{LC}/T_{LC}^\infty - \Delta H_{LM}/T_{LM}^\infty.\end{aligned} \quad (12)$$

Since A_d and V_d are proportional to d^2 and d^3, respectively, the transformation temperatures between the phases with a finite size, d, are given from eqs 9−11 by

$$d^{-1} = \Delta H_{LC}(T_{LC}^\infty - T_{LC})/C\delta_{LC}T_{LC}^\infty \quad (13)$$

$$d^{-1} = \Delta H_{LM}(T_{LM}^\infty - T_{LM})/C\delta_{LM}T_{LM}^\infty \quad (14)$$

$$d^{-1} = \Delta H_{MC}(T_{MC}^\infty - T_{MC})/C\delta_{MC}T_{MC}^\infty \quad (15)$$

where T_{LC} (= $T_m(d)$), T_{LM} and T_{MC} are L−C, L−M, and M−C transition temperatures, respectively, of the nodule structure with d and C is a constant ($A_d/V_d = Cd^{-1}$). Equation 13 is the same as eq 2 when the nodule size is replaced by the lamellar thickness (C = 2). The relations between d and the transition temperatures eqs 13−15 are summarized in Figure 14 which shows the temperature versus d^{-1} phase diagram.

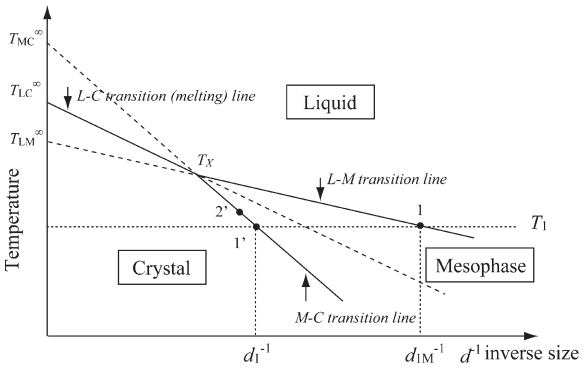

Figure 14. Temperature, T, versus inverse nodule size, d^{-1}, phase diagram obtained from the free energy with the nodule size effect in Figure 13.

When a polymer material in the system crystallizes at T_1 ($< T_{LM}^\infty$) from the glassy or molten state, the system passes through the mesomorphic phase first (Figure 13a). The mesomorphic nodules formed at T_1 grow up and transform into the crystalline nodules at $d = d_1$ where $G_M(d_1) = G_C(d_1)$ where d_n is the size of the crystalline nodule at a temperature T_n. In Figure 14, the material annealed at T_1 first forms the mesomorphic nodules of d_{1M} (at point 1), the nodules grow up to d_1, and transform into the crystalline nodules. Identical digits are used to label identical states in Figure 13 and Figure 14. When the material crystallized at T_1 is cooled to $T_{1"}$, the d at $T_{1"}$ remains d_1 because the lowest free energy of the nodule is $G_C(d_1)$. However when the nodule is heated up to T_2 ($> T_1$), the lowest free energy of the nodule becomes $G_M(d_1)$ above T_1, and the d increases and become d_2 where $G_C(d_2) = G_M(d_2)$ at T_2 (Figure 13b). The numeric marks 1′ and 2′ in Figure 13b indicates the crossing points of $G_C(d_1)$ and $G_M(d_1)$, and of $G_C(d_2)$ and $G_M(d_2)$. In Figure 13c the extrapolation line of the marks 1′ and 2′ indicate the M−C transition line (eq 15) and passes through the T_{MC}^∞. The formation mechanism of the nodule structure changes at the crossing temperature T_X where the M−C transition line intersects with G_L. Figure 14 also shows that the temperature

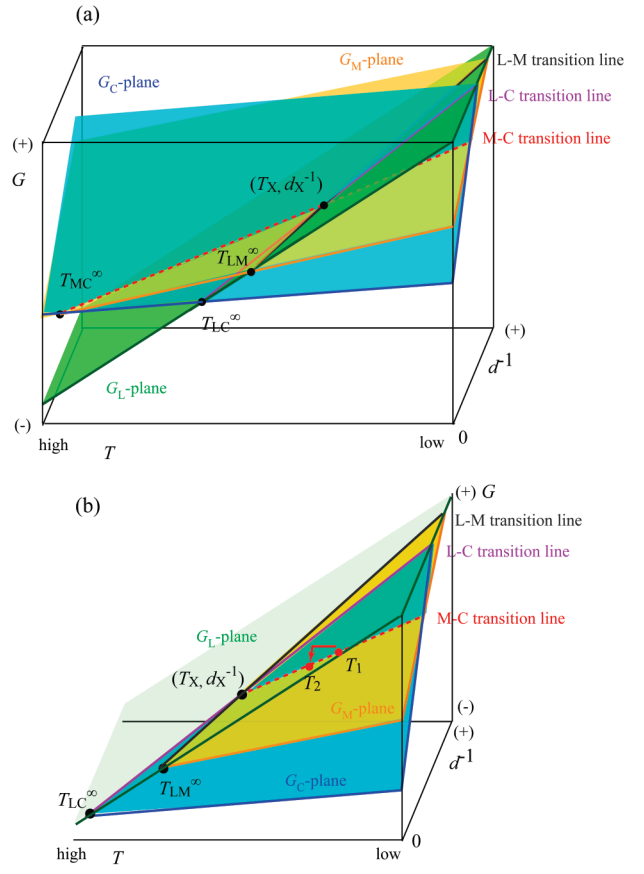

Figure 15. Schematic relationship between free energy G, temperature T and inverse characteristic nodule size, d^{-1}, for the crystalline polymer system having a metastable mesomorphic phase. Key: (a) overall view and (b) enlarged image of G_M and G_C below G_L. The arrow in part b indicates that a nodule grows by heating from T_1 to T_2 in Figures 13 and 14.

dependence of the nodule size below and above the T_X are M-C and L-C transition lines, respectively. When $T = T_{LC} = T_{LM} = T_{MC} = T_X$ in eq 12-15, d becomes d_X and the relation between T_X and the other parameters is given by

$$\delta_{MC}/(T_{MC}^{\infty} - T_X) = \delta_{LC}/(T_{LC}^{\infty} - T_X) - \delta_{LM}/(T_{LM}^{\infty} - T_X) \quad (16)$$

Figure 15 shows a schematic 3-dimensional image of G, T, and d^{-1} for the system having the mesomorphic phase as a metastable state. The lines of intersection of G_L and G_M planes, G_L and G_C planes and G_M and G_L planes are L−C, L−C, and M−C transition lines, respectively. The projections of L−M, L−C and M−C transition lines onto the $G-T$ plane give Figure 13, and the projections of L−M, L−C, and M−C transition lines onto $T-d^{-1}$ plane give Figure 14. Figure 15b shows the schematic image of G_M and G_C below G_L and clearly indicates the growth of nodule on heating from T_1 to T_2 in the same way as shown in Figure 13 and 14. Thus, the nodule grows along the M−C transition line by heating up to T_X, and grows along L-C transition line from T_X to T_{LC}^{∞}.

We apply the model to the present experimental results of PBT. In PBT, we obtain the extrapolated temperature at 330 or 333 °C, which is ca. 85 °C higher than $T_{LC}^{\infty} = 245$ °C, from the crystallization temperature dependences of the nodule size (Figure 4) and of the melting temperature of the nodule (Figure 11) between 100 and 200 °C. Furthermore, the crossing point of two temperature dependences of the q_{max} value in Figure 5 is located at 215 °C. We suggest that T_{LC}^{∞} and T_{MC}^{∞} for PBT are 245 and 333 °C, respectively. Although the accurate value of T_X is not obtained because the nodule structure can not be scaled above 200 °C from the SAXS results, we also suggest that the temperature T_X is located at ca. 215 °C. We suggest that the reason for the breakdown of the scaling of the nodule structure above 200 °C (Figures 5 and 8) near T_m^{∞} is that the nodule structure grows gradually from the size given from eq 15 in order to decrease surface energy from the DSC results (Figure 12).

Finally, we consider a possible origin of the transient mesomorphic phase for PBT. Konishi et al. have investigated the structure of the mesomorcphic phase of iPP from the viewpoint of the formation mechanism and the crystallization mechanism of iPP from the smectic structure.[19] The structure of the mesomoprhic phase has been explained liquid crystal like structure, i.e. a smectic structure by regarding the 3/1 helix as a mesogen.[19] The morphology of the smectic structure is nodular and the smectic structure transforms into α-crystalline form with the nodular morphology by heating, the size of which increases with increasing annealing temperature. Two kinds of temperature dependence of the nodule size in the crystallization from the smectic structure below and above $T_c = 125$ °C exist and lead $T_c^{\infty} = 270$ and 193 °C, respectively.[36] $T_c^{\infty} = 193$ and 270 °C and $T_c = 125$ °C correspond to T_{LC}^{∞}, T_{MC}^{∞} and T_X which are based on the modified Strobl's model, respectively. It has been confirmed that the smectic structure disappears above 125 °C by WAXD.[36] PBT also has the smectic structure by stretching the glass at room temperature. Because the smectic structure also transforms into α-crystalline form with increasing temperature above T_g, the smectic structure is a mobile metastable phase. Thus, the smectic structure may play a role of a transient mesomorphic phase in PBT.

4. Conclusion

The crystallization from the glass of PBT has been investigated by SAXS and DSC. The SAXS intensity curve of the PBT shows a long spacing of the nodular crystals of ca. 10 nm. The peak position in the SAXS curves shifts to the lower q-side with increasing annealing temperature; the nodule size increases with increasing annealing temperature. The relation between the nodule size and annealing temperature leads two extrapolated temperatures T_c^{∞}. Two linear relations between the nodule size and temperature below and above $T_c = 200$ °C lead $T_c^{\infty} = 331$ and 245 °C, respectively. The lower $T_c^{\infty} = 245$ °C corresponds to the equilibrium melting temperature T_m^{∞}. The DSC results combined with the SAXS results also show the relation between the nodule size and the melting temperature, and the relation also leads two equilibrium melting temperatures $T_m^{\infty} = 334$ °C above 245 °C. The higher $T_c^{\infty} = 330$ °C is regarded as the equilibrium mesomorphic−crystalline phase transition temperature on the basis of Strobl's crystallization model.[38] Furthermore, the change of the ratio of the nodule size to the internodule distance below 100 °C and above 200 °C is revealed by considering the normalized SAXS curve and the T_m behavior of DSC results. Below 100 °C the rigid−amorphous fraction exists around the nodule crystalline structure and inhibits the nucleation of the crystal around the nodule. Above 200 °C near T_m^{∞}, the nodule structure gradually grows in order to decrease the surface energy.

Acknowledgment. We thank Prof. K. Fukao, Ritsumeikan University, for the use of temperature controller for SAXS

measurements. We also thank Mr. Y. Yokoyama and Mr. N. Mitsuoka, Kyoto University, for their help of SAXS measurements. This work was partly supported by KAKENHI (Grant-in-Aid for Scientific Research) from the Ministry of Education, Culture, Sports, Science, and Technology of Japan, and the Core-stage backup grant of Kyoto University.

References and Notes

(1) Mencik, Z. *J. Polym. Sci. Polym. Phys. Ed.* **1975**, *13*, 2173–2181.
(2) Jakeways, R.; Ward, I. M.; Wilding, M. A.; Hall, I. H.; Desborough, I. J.; Pass, M. G. *J. Polym. Sci., Polym. Phys. Ed.* **1975**, *13*, 799–813.
(3) Joly, A. H.; Nemoz, G.; Douillard, A.; Vallet, G. *Makromol. Chem.* **1975**, *176*, 479–494.
(4) Yokouchi, M.; Sakakibara, Y.; Chatani, Y.; Tadokoro, H.; Tanaka, T.; Yoda, K. *Macromolecules* **1976**, *9*, 266–273.
(5) Hall, I. H.; Pass, M. G. *Polymer* **1976**, *17*, 807–816.
(6) Desborough, I. J.; Hall, I. H. *Polymer* **1977**, *18*, 825–830.
(7) Nitzsche, S. A.; Wang, Y. K.; Hsu, S. L. *Macromolecules* **1992**, *25*, 2397–2400.
(8) Song, K. *J. Appl. Polym. Sci.* **2000**, *78*, 412–423.
(9) Bonart, R. *Kolloid-Z.* **1966**, *213*, 1–11.
(10) Asano, T.; Seto, T. *Polym. J.* **1973**, *5*, 72–85.
(11) Auriemma, F.; Corradini, P.; de Rosa, C.; Guerra, G.; Petraccone, V.; Bianchi, R.; Dino, G. D. *Macromolecules* **1992**, *25*, 2490–2497.
(12) Asano, T.; Balta-Calleja, F. J.; Flores, A.; Tanigaki, M.; Mina, M. F.; Sawatari, C.; Itagaki, H.; Takahashi, H.; Hatta, I. *Polymer* **1999**, *40*, 6475–6484.
(13) Fukao, K.; Koyama, A.; Tahara, D.; Kozono, Y.; Miyamoto, Y.; Tsurutani, N. *J. Macromol. Sci.* **2003**, *B42*, 717–731.
(14) Jakeways, R.; Klein, J. L.; Ward, I. M. *Polymer* **1996**, *37*, 3761–3762.
(15) Konishi, T.; Nishida, K.; Matsuba, G.; Kanaya, T. *Macromolecules* **2008**, *41*, 3157–3161.
(16) Natta, G.; Corradini, P. *Nuovo Cimento* (*Suppl.*) **1960**, *15*, 40–51.
(17) Miyamoto, Y.; Fukao, K.; Yoshida, T.; Tsurutani, N.; Miyaji, H. *J. Phys. Soc. Jpn.* **2000**, *69*, 1735–1740.
(18) Minami, S.; Tsurutani, N.; Miyaji, H.; Fukao, K.; Miyamoto, Y. *Polymer* **2004**, *45*, 1413–1416.
(19) Konishi, T.; Nishida, K.; Kanaya, T.; Kaji, K. *Macromolecules* **2005**, *38*, 8749–8754.
(20) Nakaoki, T.; Ohira, Y.; Hayasi, H.; Horii, F. *Macromolecules* **1998**, *31*, 2705–2706.
(21) Ohira, Y.; Horii, F.; Nakaoki, T. *Macromolecules* **2000**, *33*, 5566–5573.
(22) Auriemma, F.; De Rosa, C.; Corradini, P. *Adv. Polym. Sci.* **2005**, *181*, 1−74 and references therein.
(23) Pyda, M.; Nowak-Pyda, E.; Heeg, J.; Huth, H.; Minakov, A. A.; Di Lorenzo, M. L.; Schick, C.; Wunderlich, B. *J Polym. Sci., Part B: Polym. Phys.* **2006**, *44*, 1364–1377.
(24) Stein, R. S.; Misra, A. *J. Polym. Sci., Polym. Phys. Ed.* **1980**, *18*, 327–342.
(25) Misra, A.; Garg, S. N. *J. Polym. Sci., Polym. Lett. Ed.* **1982**, *20*, 121–125.
(26) Matsuo, M.; Geshi, K.; Moriyama, A.; Sawatari, C. *Macromolecules* **1982**, *15*, 193–202.
(27) Runt, J.; Du, L.; Martynowicz, L. M.; Brezny, D. M.; Mayo, M. *Macromolecules* **1989**, *22*, 3908–3913.
(28) Lorenzo, M. L. D.; Righetti, M. C. *Polym. Eng. Sci.* **2003**, *43*, 1889–1894.
(29) Yoshioka, T.; Fujimura, T.; Manabe, N.; Yokota, Y.; Tsuji, M. *Polymer* **2007**, *48*, 5780–5787.
(30) Hou, P. T.; Cebe, P.; Capel, M. *J. Polym. Sci., Part B: Polym. Phys.* **1992**, *30*, 1459–1468.
(31) Hsiao, B. S.; Wang, Z.; Yeh, F.; Gao, Y.; Sheth, K. C. *Polymer* **1999**, *40*, 3515–3523.
(32) Cheng, S. Z. D.; Pan, R.; Wunderlich, B. *Macromol. Chem.* **1988**, *189*, 2443–2458.
(33) Ogawa, T.; Miyaji, H.; Asai, K. *J. Phys. Soc. Jpn.* **1985**, *54*, 3668–3670.
(34) Hsu, C. C.; Geil, P. H.; Miyaji, H.; Asai, K. *J. Polym. Sci., Part B: Polym. Phys.* **1986**, *24*, 2379–2401.
(35) Grubb, D. T.; Yoon, D. Y. *Polym. Commun.* **1986**, *27*, 84–88.
(36) Konishi, T.; Nishida, K.; Kanaya, T. *Macromolecules* **2006**, *39*, 8035–8040.
(37) Strobl, G. *Eur. Phys. J. E* **2000**, *18*, 165–183.
(38) Strobl, G. *Eur. Phys. J. E* **2005**, *18*, 295–309.
(39) Manabe, N.; Yokota, Y.; Minami, H.; Uegomori, Y.; Komoto, T. *J. Electron Microsc.* **2002**, *51*, 11–19.
(40) Strobl, G. *The Physics of Polymer*; Springer-Verlag: Berlin, 1997.
(41) Sadler, D. M.; Gilmer, G. H. *Phys. Rev. B* **1988**, *38*, 5684–5693.
(42) Janimak, J. J.; Cheng, S. Z. D.; Giusti, P. A.; Hsieh, E. T. *Macromolecules* **1991**, *24*, 2253–2260.
(43) Hauser, G.; Schmidtke, J.; Strobl, G. *Macromolecules* **1998**, *31*, 6250–6258.
(44) Heck, B.; Hugel, T.; Iijima, M.; Sadiku, E.; Strobl, G. *New J. Phys.* **1999**, *1*, 17.1–17.29.
(45) Iijima, M.; Strobl, G. *Macromolecules* **2000**, *33*, 5204–5214.
(46) Meyer, H.; Muller-Plathe, F. *J. Chem. Phys.* **2001**, *115*, 7807–7810.
(47) Reith, D.; Meyer, H.; Muller-Plathe, F. *Macromolecules* **2001**, *34*, 2335–2345.
(48) Rastogi, S.; Hikosaka, M.; Kawabata, H.; Keller, A. *Macromolecules* **1991**, *24*, 6384–6391.
(49) Keller, A.; Hikosaka, M.; Rastogi, S.; Toda, A.; Barham, P. J.; Goldbeck-Wood, G. *J. Mater. Sci.* **1994**, *29*, 2579–2604.